論文 / 著書情報
Article / Book Information

論題(和文)	
Title(English)	Directional Normalized Energy Stability Margin
著者(和文)	LAZARENKOEVGENY, 広瀬茂男, 遠藤玄
Authors(English)	Evgeny Lazarenko, SHIGEO HIROSE, Gen Endo
出典(和文)	, , ,
Citation(English)	, , ,
発行日 / Pub. date	2012, 11
Note	Proceedings of The Second IFToMM ASIAN Conference on Mechanism and Machine Science, 10. 7, 2012,- 10. 10, 2012, Tokyo, Japan, への掲載物である

Directional Normalized Energy Stability Margin

Shigeo HIROSE, Evgeny LAZARENKO, Gen ENDO *

A new approach, denoted as **DNESM** S_θ, to estimation of stability of multi-legged robots is suggested. The relationship between direction of the destabilizing force (e.g. strong sidewind, or any other kind of impact) influencing the robot, and stability margin is studied. Additionally, new stability margin is validated both in a simulation and experimentally. Simulation results correspond well with the results of experimental validation.

Keywords: *directional normalized stability margin, stability margin, directional stability*

1. Introduction

Through the past several decades a lot of researches were focused on the issue of stability of legged locomotion. The majority of scholars concentrated their efforts on studying static stability of multilegged vehicles with an assumption that stability margin can be represented by the minimum numerical value for a given supporting polygon.

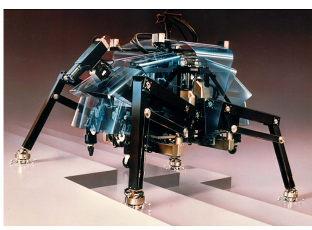

(a) TITAN IV.

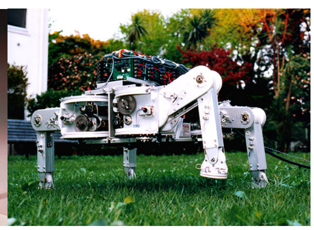

(b) TITAN VIII.

Fig.1: Robots from Hirose-Fukushima Laboratory.

In our previous works on various walking robots, examples of which are presented on fig. 1, we came to the conclusion that conventional approach to stability may be improved.

Studies about the static walks were aimed on generation of an efficient terrain-adaptive leg motion sequence, while maintaining the center of gravity (CG) of the body inside the supporting polygon. For example, static stability in fig. 2 case is defined by the shortest distance r_{23}, or by height of the potential barrier h_{23}. There were no criteria that would deal with stability in all directions, and properly consider tumbling motion and footholds located on a 3-dimentional uneven terrain.

In this paper we suggest that the concept of traditional Normalized Energy Stability Margin can be reworked in a way that turns it into a higlhy usable and versatile criterion which allows not only to define the stability in relation to a given edge of the supporting polygon, but also to define robot's stability in a given *direction* of external disturbance.

*S. Hirose, E. Lazarenko, and G. Endo are with the Dept. of Mechanical and Aerospace Engineering, Tokyo Institute of Technology, 2-12-1 Ookayama, Meguro-ku, Tokyo, 152-8550, JAPAN, hirose@mes.titech.ac.jp, lazarenko.e.aa@m.titech.ac.jp, gendo@mes.titech.ac.jp

2. Directional Normalized Energy Stability Margin

2.1 Previously Suggested Stability Criteria

2.1.1 Static Stability Margin

Stability-driven approach to multi-legged locomotion was suggested by McGhee in 1968 in a theorem that described a criterion which was later called "Static Stability Margin".

"An ideal legged locomotion machine supported by a stationary horizontal plane surface is statically stable at time t if and only if the vertical projection of the center of gravity of the machine onto the supporting surface lies within its support pattern at the given time"(fig. 2)[1].

Thus, the definition of SSM is as follows: "the magnitude of the *static stability margin* at time t for an arbitrary support pattern is equal to the shortest distance from the vertical projection of the center of gravity to any point on the boundary of the support pattern. If the pattern is statically stable, the stability margin is positive. Otherwise, it is negative." [1]

If S_{static} is positive (fig. 2), it can be calculated as

$$S_{static} = min(r_{12}, r_{23}, r_{31}), \quad (1)$$

where $r_{i,i+1}$ are the distances from robot's CG to the rotation axes around which robot performs a tumbling motion, the edges of the supporting polygon connecting P_i and P_{i+1} foothold.

SSM laid the foundations of stability-driven approach to legged locomotion and fueled subsequent researches in the field.

2.1.2 Energy Stability Margin

Proposed by Messuri and Klein [2], ESM may be formulated as the minimum potential energy, needed

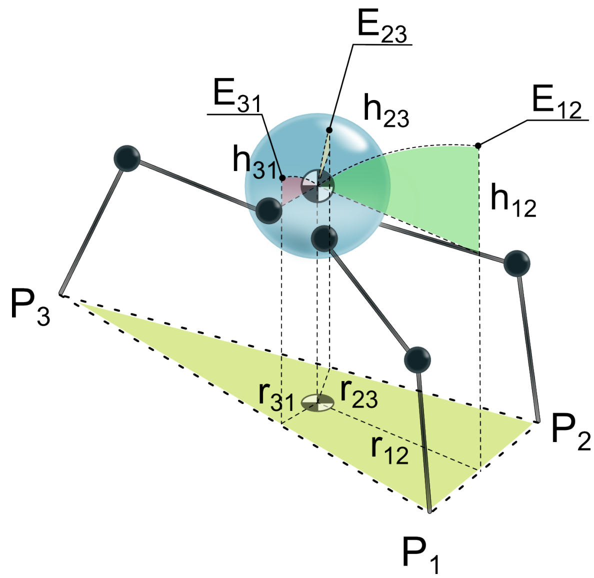

Fig.2: SSM, ESM, and NESM for a posture with a triangle as a supporting polygon. $E_{i,i+1}$ is potential energy which must be supplied to the system in order to overturn it around edge connecting P_i and P_{i+1} footholds, $h_{i,i+1}$ is the height of a corresponding potential barrier, and $r_{i,i+1}$ is the distance from CG projection to $P_{i,i+1}$ edge.

to overturn the robot around the edge of the supporting polygon (fig. 2):

$$S_{ESM} = \min_{i=1\dots n_s}(mgh_{i,i+1}) = min(E_{12}, E_{23}, E_{31}), \tag{2}$$

where mg is robot's weight, $i, i+1$ referres to $P_{i,i+1}$ edge, n_s is total number of edges of a supporting polygon, and $h_{i,i+1}$ is the variation of CG height at the time of its rotation around one of the edges of the supporting polygon, $E_{i,i+1}$ is potential energy which must be supplied to the system in order to overturn it around $P_{i,i+1}$, the edge formed by i and $i+1$ footholds.

Thus, ESM is an effective stability margin that provides qualitative estimation of the input energy that needs to be supplied to the legged vehicle system in order overturn it.

2.1.3 Normalized Energy Stability Margin

Proposed by Hirose *et al.*, is represented as

$$S_{NESM} = \frac{S_{ESM}}{mg} = \min_{i=1\dots n_s}(h_{i,i+1}), \tag{3}$$

or ESM normalized to robot's weight [3] and represented by the height of a potential barrier (fig. 2) to an unstable equilibrium above the edge of the supporting polygon, i.e. tumbling. Real experiments on the model of a quadruped robot standing on a slope proved that NESM is the most accurate stability margin for evaluation of stability of walking vehicles.

Not only it possesses all the advantages of ESM, but also provides a way to compare stability of different types of multi-legged robots.

2.1.4 Normalized Dynamic Energy Stability Margin

Another branch of legged vehicles stability science is normalized dynamic enegy stability margin. Previously suggested criteria rarely consider any dynamic effects that could cause robot's instability, but an important milestone in this direction is "Normalized Dynamic Energy Stability Margin", or NDESM. Proposed by De Santos *et al.* [4, 5], NDESM was designed to account for inertial forces and manipulation effects occuring during robot's motion, and can be formulated as "the smallest of the stability levels required to tumble the robot around the support polygon, normalized to the robot's mass, accounting for robot/ground interaction forces".

While providing an estimation of the influence of dynamic effects of a mounted arm on stability, NDESM does not completely account for external destabilizing factors (e.g. strong side wind or sudden strike, etc.), thus being only a partial extension of NESM.

2.2 Extended Normalized Energy Stability Margin

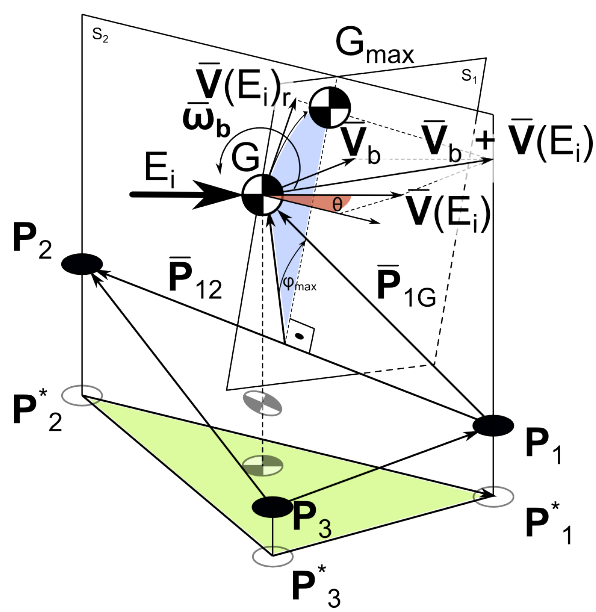

Fig.3: CG rotation around the edge of the supporting polygon. (See below for the definitions of the parameters depicted on the figure.)

If we think about destabilized motion of walking robot's CG, it always occurs in presense of a certain external force applied to robot. That force obviously has a direction, although in previous formulations of stability criteria tumbling motion in the direction of external disturbance was not considered in any way.

We propose **Directional Normalized Energy Stability Margin (DNESM), or** S_θ, defined as the minimum amount of input energy E_i applied in the form of horizontal force with a yaw anglular direction θ required to tumble an object, divided by the weight mg of the object itself. Proposed DNESM S_θ is expressed as follows:

$$S_\theta = \left.\frac{E_i}{mg}\right|_\theta . \tag{4}$$

In this criterion we assume the phenomenon of instanteneous time, when robot's movement is measured in descreete time snapshots, therefore, even though $\mathbf{V}(E_i)$ is created by a certain input force which is, in turn, caused by an input energy E_i, we may neglect such parameters as acceleration under the influence of that force, feet slipping, etc. Input energy E_i is applied to the center of gravity of the object in the form of force $\mathbf{F}(E_i)$ that acts in the horizontal plane on the yaw angle θ and generates velocity $\mathbf{V}(E_i)$.

We also assume that the application of input energy E_i to the object is done at a time t while CG of the object is making a motion with velocity $\mathbf{V}_b$ and angular velocity $\boldsymbol{\omega}_b$, and as soon as input energy E_i is applied, the internal motion of the object is frozen and the object starts a new motion with velocity $\mathbf{V}_b + \mathbf{V}(E_i)$ and angular velocity $\boldsymbol{\omega}_b$.

As the dimension of the stability criterion S_θ is "length", it can be considered to be the height of potential barrier of the object formed to the horizontal direction θ against input disturbance energy.

$\mathbf{S}_\theta$ inherits both NESM's and NDESM's usability, acting as a measure of margin length and accounting for parameters of robot's motion, and equips us with a method of more precise stability estimation, showing that multilegged vehicles' stability is not just a level of minimum energy required to overturn the robot, but a level of minimum energy, *applied in a certain direction*, that may overturn the robot around the edge of the supporting polygon.

3. Derivation of DNESM

3.1 Tumbling Motion Analysis

To clarify the derivation process, let us analyze tumbling motion of a walking robot. In this paper we only consider the case of an n-legged supporting polygon, and we do not account for the effect of the swinging legs. Tumbling-prevention, including the effect of the swinging legs, will be discussed in the following publications.

Let us consider the case of a 3 leg supported walking robot with no swinging legs, standing on an uneven terrain, and its movement in presence of a certain input energy E_i that is applied in the form of horizontal input velocity $\mathbf{V}(E_i)$ ($V(E_i) = \sqrt{2E_i/m}$) of the CG (Fig. 3). P_1, P_2, P_3 are ground contact points, while P_1^*, P_2^*, P_3^* are their projections on a horizontal plane.

Destabilizing energy E_i is supplied to the system in order to overturn the robot. Main condition for overturning is moving robot's CG from its current stable position G to a position G_{max} – an unstable equilibrium in rotation around P_1P_2 edge of the supporting polygon.

In order to derive S_θ, let us consider the case when robot's CG experiences a rotation around P_1P_2 edge (fig. 3), produced by means of an external input velocity $\mathbf{V}(E_i)$ applied in a horizontal plane. Yaw direction θ of $\mathbf{V}(E_i)$ is variable, and magnitude of $\mathbf{V}(E_i)$ is defined by the amount of energy required to overturn the robot.

Let us define all necessary variables and derive $\mathbf{V}(E_i)$ magnitude, as shown on Fig. 3. First, we shall derive the rotational velocity $\mathbf{V}(E_i)_r$ generated by the input velocity $\mathbf{V}(E_i)$.

Footholds of the supporting polygon and CG of the robot may be written as $P_i(x_i, y_i, z_i), i = 1 \dots 3$, and $G(x_G, y_G, z_G)$.

Vector $\mathbf{P}_{12}$ from P_1 to P_2 is expressed as

$$\mathbf{P}_{12} = (x_2 - x_1, y_2 - y_1, z_2 - z_1)^T, \tag{5}$$

and its unit vector $\hat{\mathbf{P}}_{12}$

$$\hat{\mathbf{P}}_{12} = \frac{1}{\|P_{12}\|}\begin{bmatrix} x_2 - x_1 \\ y_2 - y_1 \\ z_2 - z_1 \end{bmatrix}, \tag{6}$$

where

$$\|P_{12}\| = \sqrt{(x_2 - x_1)^2 + (y_2 - y_1)^2 + (z_2 - z_1)^2}. \tag{7}$$

Vector $\mathbf{P}_{1G}$ from P_1 to G is expressed as

$$\mathbf{P}_{1G} = (x_G - x_1, y_G - y_1, z_G - z_1)^T, \tag{8}$$

and its unit vector $\hat{\mathbf{P}}_{1G}$ is expressed as

$$\hat{\mathbf{P}}_{1G} = \frac{1}{\|P_{1G}\|}\begin{bmatrix} x_G - x_1 \\ y_G - y_1 \\ z_G - z_1 \end{bmatrix}, \tag{9}$$

where

$$\|P_{1G}\| = \sqrt{(x_G - x_1)^2 + (y_G - y_1)^2 + (z_G - z_1)^2}. \tag{10}$$

The unit vector $\hat{\mathbf{V}}_{12G}$ of transverse velocity of CG's rotation around $\mathbf{P}_{12}$ can be written as:

$$\hat{\mathbf{V}}_{12G} = \hat{\mathbf{P}}_{12} \times \hat{\mathbf{P}}_{1G}, \tag{11}$$

$$\hat{\mathbf{V}}_{12G} = \frac{\begin{vmatrix} i & j & k \\ x_2 - x_1 & y_2 - y_1 & z_2 - z_1 \\ x_G - x_1 & y_G - y_1 & z_G - z_1 \end{vmatrix}}{\|\mathbf{P}_{12}\|\|\mathbf{P}_{1G}\|}, \tag{12}$$

$$\hat{\mathbf{V}}_{12G} = \frac{\mathbf{A}_{12}}{\|\mathbf{P}_{12}\|\|\mathbf{P}_{1G}\|}, \tag{13}$$

where

$$\mathbf{A}_{12} = \begin{bmatrix} (y_2 - y_1)(z_G - z_1) - (y_G - y_1)(z_2 - z_1) \\ -(x_2 - x_1)(z_G - z_1) + (x_G - x_1)(z_2 - z_1) \\ (x_2 - x_1)(y_G - y_1) - (x_G - x_1)(y_2 - y_1) \end{bmatrix}. \tag{14}$$

At the same time, let us express horizontal input velocity as

$$\mathbf{V}(E_i) = (V(E_i)\cos\theta, V(E_i)\sin\theta, 0)^T. \tag{15}$$

Then, rotational velocity $\mathbf{V}(E_i)_r$ of the CG around vector $\mathbf{P}_{12}$ caused by the input velocity $\mathbf{V}(E_i)$ can be expressed as

$$\mathbf{V}(E_i)_r = \big(\mathbf{V}(E_i) \cdot \hat{\mathbf{V}}_{12G}\big)\hat{\mathbf{V}}_{12G}, \tag{16}$$

By substituting equations (13) and (15) parameters of equation (16) can be expressed as

$$\mathbf{V}(E_i) \cdot \hat{\mathbf{V}}_{12G} = \frac{V(E_i)B_{12}}{\|\mathbf{P}_{12}\|\|\mathbf{P}_{1G}\|}, \tag{17}$$

where

$$\begin{aligned} B_{12} = \Big[&\big((y_2 - y_1)(z_G - z_1) - \\ &- (y_G - y_1)(z_2 - z_1)\big)\cos\theta + \\ &+ \big(-(x_2 - x_1)(z_G - z_1) + (x_G - x_1)(y_2 - y_1)\big)\sin\theta\Big]. \end{aligned} \tag{18}$$

Therefore, rotational velocity of CG generated by the input velocity $\mathbf{V}(E_i)$ can be expressed as

$$\mathbf{V}(E_i)_r = \frac{V(E_i)B_{12}}{\|\mathbf{P}_{12}\|^2\|\mathbf{P}_{1G}\|^2}\mathbf{A}_{12}. \tag{19}$$

Next, we have to define a top point G_{max} which CG can reach in its rotation around $\mathbf{P}_{12}$, the point of maximum potential energy and unstable equilibrium above P_1P_2 edge. It is known that rotated vector $\mathbf{R}$ around vector $\boldsymbol{\omega}$ on angle φ (Fig. 4) can be expressed as

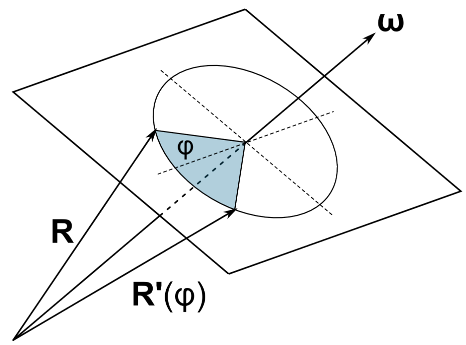

Fig.4: Vector rotation.

$$\begin{aligned} \mathbf{R}'(\varphi) =& (\mathbf{R} \cdot \boldsymbol{\omega})\boldsymbol{\omega} + \cos\varphi(\mathbf{R} - (\mathbf{R} \cdot \boldsymbol{\omega}) \cdot \boldsymbol{\omega}) + \\ &+ \sin\varphi(\boldsymbol{\omega} \times \mathbf{R}). \end{aligned} \tag{20}$$

This relation can be used to describe our case in a similar fashion by substituting $\mathbf{P}_{1G}$ as $\mathbf{R}$, $\hat{\mathbf{P}}_{12}$ as $\boldsymbol{\omega}$, and $\mathbf{G}(\varphi) - \mathbf{P_1}$ as $\mathbf{R}'(\varphi)$, giving us the following equation:

$$\begin{aligned} &\mathbf{G}(\varphi) = (\mathbf{P}_{1G} \cdot \hat{\mathbf{P}}_{12})\hat{\mathbf{P}}_{12} + \\ &\cos\varphi\Big(\mathbf{P}_{1G} - (\mathbf{P}_{1G} \cdot \hat{\mathbf{P}}_{12})\hat{\mathbf{P}}_{12}\Big) + \sin\varphi(\hat{\mathbf{P}}_{12} \times \mathbf{P}_{1G}) + \\ &+ \mathbf{P_1}. \end{aligned} \tag{21}$$

Here, $\mathbf{P}_{1G} \cdot \hat{\mathbf{P}}_{12}$ can be expressed from equations (8) and (11) as

$$\mathbf{P}_{1G} \cdot \hat{\mathbf{P}}_{12} = \frac{1}{\|\mathbf{P}_{12}\|}C_{12}, \tag{22}$$

where

$$\begin{aligned} C_{12} =& (x_G - x_1)(x_2 - x_1) + \\ &+ (y_G - y_1)(y_2 - y_1) + (z_G - z_1)(z_2 - z_1). \end{aligned} \tag{23}$$

And $\hat{\mathbf{P}}_{12} \times \mathbf{P}_{1G}$ is expressed from equations (13) and (15) as:

$$\mathbf{P}_{12} \times \mathbf{P}_{1G} = \frac{1}{\|\mathbf{P}_{12}\|}\mathbf{A}_{12}. \tag{24}$$

By substituting members of (21) with previously found relations, we can write a function defining the CG movement around P_1P_2 axis:

$$\mathbf{G}(\varphi) = \frac{C_{12}}{\|\mathbf{P}_{12}\|^2}\begin{bmatrix} x_2 - x_1 \\ y_2 - y_1 \\ z_2 - z_1 \end{bmatrix} + \tag{25}$$
$$+ \cos\varphi \begin{bmatrix} (x_G - x_1) - \frac{C_{12}}{\|\mathbf{P}_{12}\|^2}(x_2 - x_1) \\ (y_G - y_1) - \frac{C_{12}}{\|\mathbf{P}_{12}\|^2}(y_2 - y_1) \\ (z_G - z_1) - \frac{C_{12}}{\|\mathbf{P}_{12}\|^2}(z_2 - z_1) \end{bmatrix} +$$
$$+ \frac{\sin\varphi}{\|\mathbf{P}_{12}\|}\mathbf{A}_{12} + \mathbf{P}_1,$$

where $\mathbf{A}_{12}$ is shown in the equation (14).

Obviously, we have to find φ_{max}, the angle travelled by CG to the highest point rotation around P_1P_2. Highest position of $\mathbf{G}(\varphi)$ can be derived by the extremum of its equation of motion $\partial G(\varphi)_z/\partial\varphi = 0$, where $G(\varphi)_z$ is the z component of $\mathbf{G}(\varphi)$, and expressed as:

$$\frac{\partial G(\varphi)_z}{\partial \varphi} = -\sin\varphi_{max}\Big(z_G - z_1 - \tag{26}$$
$$- \frac{C_{12}}{\|\mathbf{P}_{12}\|^2}(z_2 - z_1)\Big) +$$
$$+ \frac{\cos\varphi_{max}}{\|\mathbf{P}_{12}\|}\Big((x_2 - x_1)(y_G - y_1) -$$
$$- (x_G - x_1)(y_2 - y_1)\Big) = 0.$$

thus, the following equation holds:

$$\frac{\sin\varphi_{max}}{\cos\varphi_{max}} = D_{12}, \tag{27}$$

where

$$D_{12} = \frac{(x_2 - x_1)(y_G - y_1) - (x_G - x_1)(y_2 - y_1)}{\|\mathbf{P}_{12}\|(z_G - z_1) - \frac{C_{12}}{\|\mathbf{P}_{12}\|}(z_2 - z_1)}. \tag{28}$$

Finally, angular distance φ_{max} can be expressed as

$$\varphi_{max} = \arctan(D_{12}). \tag{29}$$

From (29) and (21) we can define $\mathbf{G}_{max}$ as $\mathbf{G}(\varphi_{max})$, and it is expressed as

$$\mathbf{G}_{max} = \frac{C_{12}}{\|\mathbf{P}_{12}\|}\hat{\mathbf{P}}_{12} + \tag{30}$$
$$+ \cos\varphi_{max}\Big(\mathbf{P}_{1G} - \frac{C_{12}}{\|\mathbf{P}_{12}\|}\hat{\mathbf{P}}_{12}\Big) +$$
$$+ \sin\varphi_{max}\frac{\mathbf{A}_{12}}{\|\mathbf{P}_{12}\|} + \mathbf{P_1}.$$

Height difference between original CG position G and the highest position of G_{max} can be expressed as

$$H_{12} = G_{max\ z} - G_z. \tag{31}$$

Magnitude of $V(E_i)$ to move CG just to the top position G_{max} is

$$\frac{1}{2}m\|\mathbf{V}(E_i)_r\|^2 = mgH_{12}. \tag{32}$$

From (17):

$$\|\mathbf{V}(E_i)_r\|^2 = Z_{12}^2 V^2(E_i), \tag{33}$$

where Z_{12}^2 is defined as

$$Z_{12}^2 = \Big(\frac{B_{12}}{\|\mathbf{P}_{12}\|^2\|\mathbf{P}_{1G}\|^2}\Big)^2\mathbf{A}_{12}^T\mathbf{A}_{12}. \tag{34}$$

Substituting (34) to (32), relation between kinetic energy and potential energy to lift CG above the edge of the supporting polygon is expressed as

As a result, input velocity $V(E_i)$ needed to move CG to the top position above P_1P_2 edge can be expressed as

$$\frac{1}{2}mV^2(E_i) = mg\frac{H_{12}}{Z_{12}^2}. \tag{35}$$

Thus, Directional Normalized Energy Stability Margin, or S_θ, corresponding potential barrier to the input velocity in the direction θ, can be expressed as:

$$S_\theta = \frac{H_{12}}{Z_{12}^2}. \tag{36}$$

3.2 Derivation of $\mathbf{S}_\theta$ for a generalized supporting posture

In this section we will summarize a calculation of S_θ for a walking robot with an n-legged supporting posture.

We assume that a walking robot is affected by an input energy E_i that generates horizontal input velocity $\mathbf{V}(E_i)$ of the CG (Fig. 3). P_i and P_{i+1} are ground contact points.

Edges of the supporting polygon and CG of the robot may be denoted as $P_{i,i+1}(x_i, y_i, z_i), i = 1 \ldots n$, and $G(x_G, y_G, z_G)$ correspondingly.

Thus, DNESM S_θ for the edge of the supporting polygon connecting ith and $(i+1)$th foothold may be easily computed through the following algorithm.

1. Find necessary coefficients $C_{i,i+1}$, and $D_{i,i+1}$ from equations (23), and (28) correspondingly.

2. Find a maximum angular displacement of robot's CG $\varphi^{max}_{i,i+1}$ from equation (29).
3. Find coefficient $\mathbf{A}_{i,i+1}$ from (14).
4. From (30) calculate $G_{(i,i+1)max}$.
5. Calculate $H_{i,i+1}$, height difference between original CG position G and its highest possible position $G_{(i,i+1)max}$ above $(\mathbf{i}, \mathbf{i+1})$, from (31).
6. Find coefficient $B_{i,i+1}$ from (18).
7. Calculate a coefficient $Z_{i,i+1}$ for an $(\mathbf{i}, \mathbf{i+1})$ axis from (34).
8. Finally, S_θ for an $(\mathbf{i}, \mathbf{i+1})$ line of supporting polygon can be calculated as

$$S_\theta = \frac{H_{i,i+1}}{Z^2_{i,i+1}}. \tag{37}$$

It is easy to show that in a boundary case, when input energy is directed normally to the i-th edge of the supporting polygon, S_θ is minimum for this particular edge.

3.3 Initial numerical simulation

In order to perform initial validation of S_θ, we have created a numerical model for calculation of S_θ. A simulation scenario can be described in the following points:

- External energy E_i is supplied to the system in a horizontal plane, and, thus, $\mathbf{V}(E_i)$ lays in the horizontal plane as well.
- In *numerical simulation* friction in the footholds is infinite, and slipping does not occur.
- In *numerical simulation* legs are massless, and robot's mass is concentrated in the body.
- Body velocity $\mathbf{V}_b = 0$ and $\boldsymbol{\omega} = 0$ in both cases.
- Simulation and experiment are conducted on both flat and uneven surfaces.

Simulation was conducted for two cases: $P_2 = (17.5, 30.31, 0)$ and $P_2 = (17.5, 30.31, 5)$; results are shown on fig. 5.

4. Validation with an experimental setup

Equation (36) which allows us to calculate DNESM was derived with certain assumptions. In order to find out whether our assumptions are correct and how well our derivation process corresponds to a real life situation, it is required that we perform a model experiment with some kind of actual model of a robot, measuring S_θ manually, and comparing our results with a simulation for the same model.

In order to validate proposed derivation process of DNESM S_θ, we performed a simple tumbling experiment with a setup which shown on Fig. 6a. It consisisted of the following elements: a pendulum with a hammer 1 (mass: 470 g) attached to a connecting rod 2 and rotating on a shaft 3; a robot model 4 (mass: 490 g) with lightweight legs (mass of each leg 2.3g Fig.

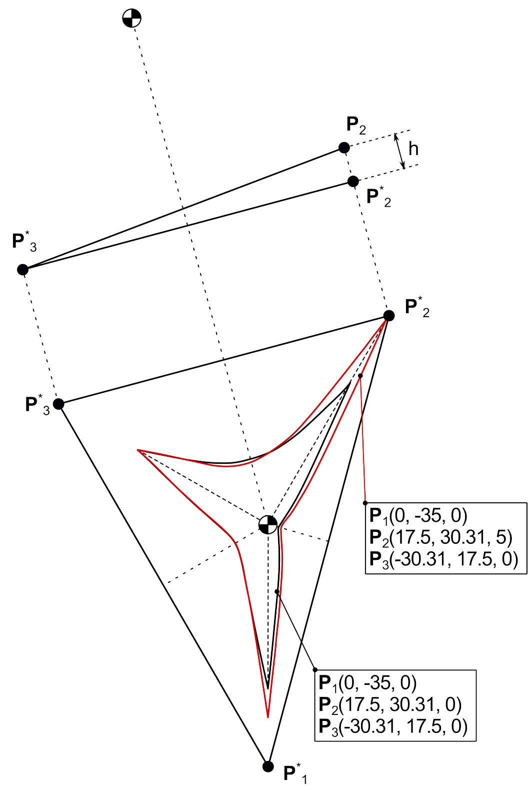

Fig.5: Calculation of S_θ for two cases (numbers are the coordinates of footholds in mm, when projection of CG on a horizontal plane is in the origin of cortesian coordinate system).

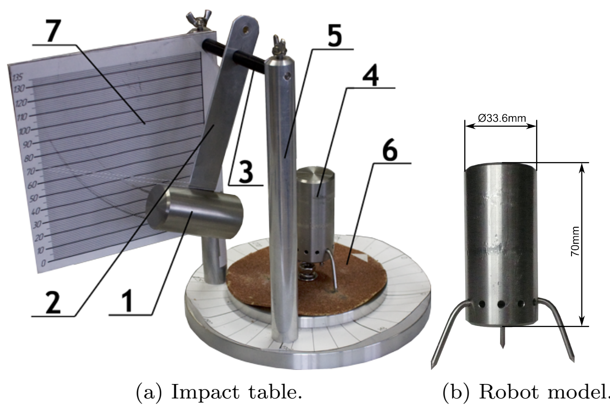

(a) Impact table. (b) Robot model.

Fig.6: Experimental setup.

6b; as mass of the legs is small compared to mass of the body, they can be neglected; supporting pillars 5; rotary table 6 for positioning the body against hammer 1, and a vertical scale 7 for measuring the value of S_θ.

Experimental process was done to measure the lowest height of the pendulum that defined a corresponding potential energy required to overturn the body. After several iterations for each angular position, we were able with a certain precision to make a measurment of S_θ.

One of the limiting factors for our work was insufficient friction of the surface of a rotary table of the experimental setup. In cases when S_θ was high, slipping of the body occured, which resulted in a lack of measurment accuracy. To solve this problem, rotary table was covered with sandpaper which significanlty improved the quality of measurements.

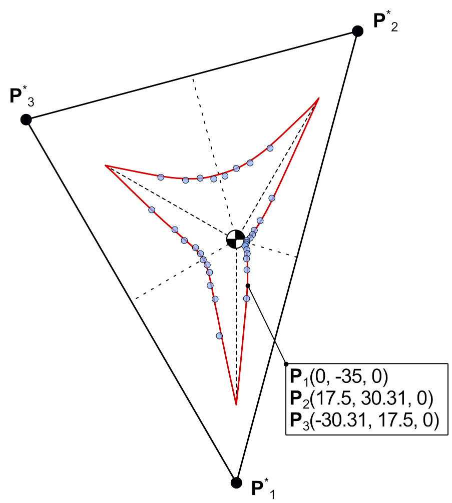

(a) Comparison of a simulation and model experiment results in case of flat ground.

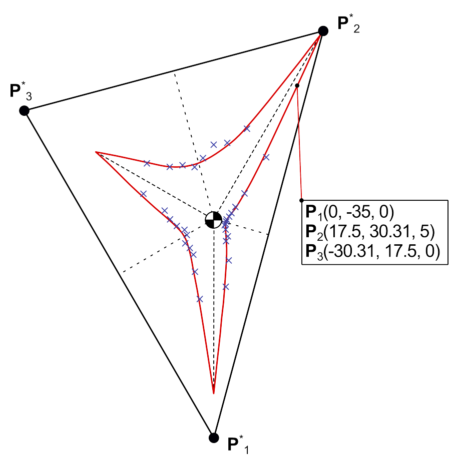

(b) Comparison of a simulation and model experiment results in case of inclined ground.

Fig.7: Overlayed results of simulation and experimental validation.

Data from the simulation and experiment were compared, and are presented on Fig. 7.

Fig. 7b demonstrates a case when leg 2 foothold is raised 5 mm above the ground.

As one can see on the graph, experimental results correspond well with the derivation results of S_θ as it was proposed in Chapter 4. That proves general validity of our proposed method.

5. Conclusion and future work

In our work we suggested **DNESM** S_θ, a new way to estimate stability of multi-legged robots. We studied the relationship between direction of the destabilizing force (e.g. strong sidewind, or any other kind of impact) influencing the robot, and stability margin. Finally, S_θ was validated both in a simulation and experimentally, and simulation results corresponded well with experimental validation.

One of the goals of our work is to show **DNESM** applicability in simulation that would account for dynamic effects, and develop a gait generation method to perform a stable gait on every type of terrain. In order to achieve this, we need to explain the derivation of DNESM S_θ considering the swinging legs. We would like to discuss these ideas in subsequent papers.

References

[1] R.B. McGhee and A.A. Frank, “On the Stability Properties of Quadruped Creeping Gaits” *Mathematical Biosciences*, vol. 3, 1968, pp. 331-351.

[2] D. A. Messuri and C.A. Klein “Automatic Body Regulation for Maintaining Stability of a Legged Vehicle During Rough-Terrain Locomotion”, *IEEE Journal of Robotics and Automation*, vol. RA-1(3), 1985, pp. 132-141.

[3] S. Hirose, H. Tsukagoshi, K. Yoneda, “Normalized Energy Stability Margin: Generalized Stability Criterion for walking vehicles”, *Proceedings of International Conference on Climbing and Walking Robot*, Brussels, Belgium, 1998, pp. 71-76.

[4] E. Garcia and P. Gonzalez de Santos,“An Improved Energy Stability Margin for Walking Machines Subject To Dynamic Effects”, *Robotica*, vol. 23, Cambridge University Press, 2005, pp. 13-20.

[5] P. Gonzalez de Santos, E. Garcia, J. Estemera,“Quadrupedal Locomotion. An Introduction to the Coltrol of Four-legged Robots”, Springer; 2006.

[6] F. Gantmacher,“Lectures in Analytical Mechanics”, MIR Publications; 1975.

[7] K. Yoneda and S. Hirose, “Tumble Stability Criterion of Integrated Locomotion and Manipulation”, *Proceedings of International Conference on Intelligent Robots and Systems*, 1996, pp. 870-876.

[8] K. Yoneda and S. Hirose, “Three-Dimensional Stability Criterion of Integrated Locomotion and Manipulation”, *Journal of Robotics and Mechatronics*, vol. 9, no. 4, 1997, pp. 267-274.